J. Space Weather Space Clim. 2023, **13**, 3

https://doi.org/10.1051/swsc/2023002

JSWSC

Available online at:
www.swsc-journal.org

Topical Issue - Ionospheric plasma irregularities and their impact on radio systems

RESEARCH ARTICLE OPEN ACCESS

Field-aligned scale length of depleted structures associated with post-sunset equatorial plasma bubbles

Chao Xiong[1,2,*] and Hermann Lühr[3]

[1] Hubei Luojia Laboratory, 430079 Wuhan, China
[2] Department of Space Physics, Electronic Information School, Wuhan University, 430072 Wuhan, China
[3] GFZ German Research Centre for Geosciences, Section 2.3, Geomagnetism, Telegrafenberg, 14473 Potsdam, Germany

Received 29 June 2022 / Accepted 26 January 2023

Abstract – In this study we make use of the Swarm counter-rotation constellation for estimating the typical scale length of the post-sunset equatorial plasma bubbles (EPBs) along fluxtubes. The close approaches between Swarm spacecraft near the equator occurred in September and October 2021, covering the magnetic local time from 19:00 to 23:00, which is favorable for the occurrence of EPBs. It is the first time to show the quasi-simultaneously samplings by Swarm A/C and B of the same fluxtube but at different altitude. The observations frequently reveal plasma density depletions only at one spacecraft altitude, confirming that EPBs extend only over finite parts of the fluxtube. Based on a statistical analysis of double and single EPB detections on the same fluxtube, our results imply the typical field-aligned scale length of the depletion structures associated with EPBs of the order of 550 km. Our detections are from the lower part of the depleted fluxtubes, and they coincide well with the latitudes of the equatorial ionization anomaly. In the upper part of the fluxtube near the magnetic equator, our estimation technique does not work well because of too large field-aligned spacecraft separation of the Swarm satellites.

Keywords: Ionospheric plasma irregularities / Equatorial plasma depletions / Depleted magnetic fluxtubes / Scale-length of plasma bubbles

1 Introduction

The term post-sunset equatorial plasma bubble (EPB), or equatorial spread-F (ESF), stands for a localized region of plasma density depletion at the low-latitude ionosphere during post-sunset hours. The absence of sunlight after sunset leads to much faster recombination at a lower altitude, which causes a steep upward plasma density gradient between the depleted bottom-side ionosphere and higher density in the upper F region. This vertical plasma density gradient provides a favorable condition for the appearance of Rayleigh–Taylor instability. The instability can then rise to higher altitudes due to an enhanced $E \times B$ drift caused by the pre-reversal enhancement of the eastward electric field at sunset, and finally forms the well-developed small-scale plasma irregularities in the nighttime F region ionosphere (Heelis et al., 1974; Fejer et al., 1999; Kelley, 2009). When radio waves pass through these irregularities, their phase and amplitude will suffer random fluctuations, known as ionospheric scintillation, which further causes degraded performance of positioning and navigation signals (e.g., Yeh & Liu, 1982; Kintner et al., 2007; Xiong et al., 2016a).

Due to the large electric conductivity along magnetic field lines, the small-scale irregularities associated with EPBs are thought to be elongated along the whole depleted fluxtubes (e.g., Kelley, 2009). Earlier campaigns including observations from multi-instruments at Arecibo, Puerto Rico, revealed that the often-observed dark bands (or streaks) in the all-sky airglow images correspond well with the depleted plasma density regions (Mendillo et al., 1997). Later observations from airglow imagers at other locations show that this kind of dark band is mainly distributed along the local magnetic meridian (e.g., Mukherjee et al. 1998; Pimenta et al., 2003; Wu et al., 2017). Backward C-shaped images of EPBs, observed e.g. by the Global Ultraviolet Imager (GUVI) onboard the TIMED satellite, also suggested that the depleted plasma associated with EPBs generally follows a depletion shell (Kil et al., 2009).

Though the above-mentioned results from the airglow imagers support the assumption that the EPBs are distributed along the magnetic fluxtube, depleted structures associated with EPBs are believed to have finite scale length under some specified conditions, e.g., appearing in the neighborhood of plasma density enhancement (Le et al., 2003), or at the developing phase of EPBs (Fig. 8c of Huang et al., 2014). In a statistical sense, similar suggestions also arise from observations of

*Corresponding author: xiongchao@whu.edu.cn

near-polar orbiting satellites. As shown by Luo et al. (2019), plasma density depletions are occasionally observed only in one hemisphere, as seen in the in-situ electron density measurements of a Swarm satellite, even when the satellite track follows well the magnetic meridian in the two hemispheres. They concluded that the depletions associated with EPBs might not be symmetrically distributed along the fluxtube. Based on numerical simulations, Dao et al. (2013) pointed out that the off-equator plasma depletions are coupled remotely via Alfvén waves. Yokoyama et al. (2014) derived from their high-resolution 3D bubble model the complex evolution of depleted regions showing bifurcations and pinching in the equatorial region. A recent study by Ghadjari et al. (2022) provided evidence for standing Alfvén waves trapped within the EPBs, and the authors further estimated the field-aligned length of the EPBs within the range of 110–200 km, which is much smaller than the field line length of a fluxtube reaching from the E region into F region. However, these authors analyzed only two quite special examples of EPBs.

The main purpose of this study is to improve our understanding of the field-aligned scale length of EPBs. The basis for this analysis is the in-situ electron density (*Ne*) measurements of the Swarm satellites during the period of counter-rotation constellation when the orbital planes of all three spacecraft came close together in the low-latitude region, allowing for quasi-simultaneous observations of the same fluxtube but at two different altitudes. This occurred during September and October 2021 and covered right the post-sunset hours. Based on a statistical study we try to obtain the field-aligned scale length of EPBs. The paper follows the traditional structure. First, the considered instruments and data are introduced. Subsequently, the observations are presented and the obtained results are discussed. Finally, the main results are summarized and conclusions are drawn.

2 Swarm satellites and the constellation evolution

ESA's Earth observation mission Swarm was launched on 22 November 2013. It consists of three identical satellites in near-polar orbits at different altitudes. During the first mission phase, starting on 17 April 2014, Swarm A and C fly side-by-side, separated at 1.4° in longitude, at an altitude of about 460 km and an inclination of 87.3°. Swarm B is orbiting the Earth at about 50 km higher with an inclination of 88°. This difference in inclination causes a slowly increasing difference in longitude between the two orbital planes amounting to about 2° per month.

Each of the three satellites is equipped with a set of six instruments (Friis-Christensen et al., 2008). In this study, we use the data from the Swarm Langmuir Probe (LP) which is part of the Electric Field Instrument (EFI) package, and a detailed description of EFI can be found in Knudsen et al. (2017). Plasma densities are derived by the LP at a time resolution of 2 Hz.

During the second mission phase, starting in October 2019, the separation between Swarm A and C was slowly reduced. After almost 8 years in orbit a counter-rotating, the quasi coplanar configuration was achieved between all three, the

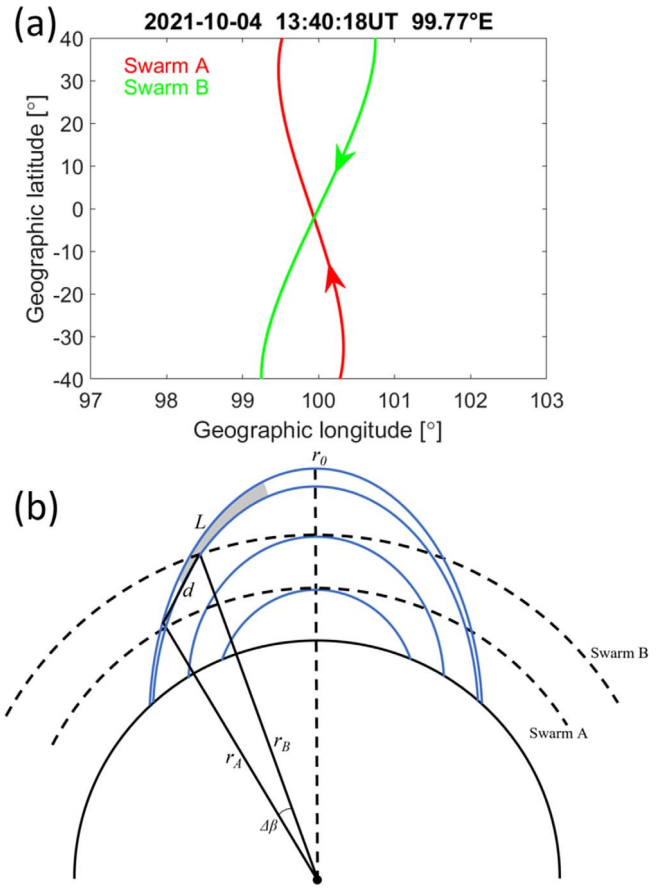

Figure 1. (a) One example of Swarm A and B ground tracks during the period of counter-rotation in geographic coordinates. Arrows indicate the flying direction of the two satellites. (b) Relation between three selected dipole field lines (blue solid lines) and the orbits of Swarm A and B (black dashed lines). The third black line, marked by *d*, is a fluxtube segment bounded by the two orbits. The grey-shading segment within the highest fluxtube represents the depleted structures of EPBs with a field-aligned scale length of *L*, which is encountered by Swarm B but not by the lower-flying Swarm A.

Swarm A/C pair and Swarm B. Around 4 October 2021, the orbital planes of Swarm A/C and Swarm B crossed near the equator. Weeks before that date the crossing occurred on the ascending arcs of Swarm A/C south of the equator and weeks after in the northern hemisphere. The crossing point drifted by about 0.86° in latitude per day from south to north. This provides the closest approaches of Swarm A/C with Swarm B within the latitude range of ±20° during September and October 2021.

Figure 1a shows an example of the Swarm A and B ground tracks on 04 October 2021 in a geographic latitude versus longitude frame. During the considered two-month time interval (September and October 2021), the magnetic local time (MLT) at ascending arc of the Swarm A/C orbital plane varied from 23:00 to 18:30. This is a very favorable time sector for the appearance of post-sunset EPBs. The spacecraft crossed, during that interval, the equator at average altitudes of about 435 km for Swarm A/C and 506 km for Swarm B.

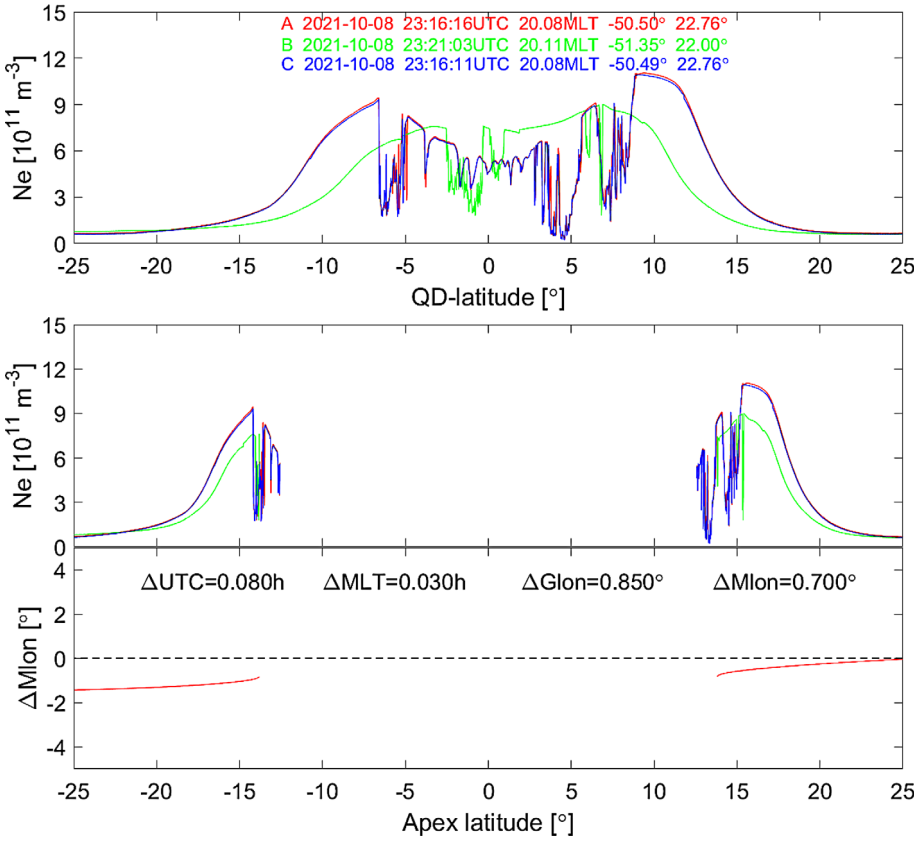

Figure 2. Example of electron density recordings by the Swarm satellites of a plasma depletion event at low latitudes. In the top frame, the plasma variations are plotted over magnetic latitude; in the bottom frame, they are showing versus the E-layer footprint of the fluxtube (ApexLat). Low-latitude fluxtubes do not reach satellite heights. In the bottom panel, the magnetic longitude difference (ΔMLon) between the Swarm A/C and Swarm B observations is shown.

It is commonly assumed that the individual plasma depletions are extended along the whole magnetic fluxtube. Therefore, simultaneous observations on the same field line are of interest for this study. Consequently, we plotted the *Ne* measurements at the two heights ordered by the common field line. To achieve that, we make use of the magnetic Apex latitudes (ApexLat) of the field lines (Emmert et al., 2010). In this system, the whole magnetic field line is labeled by its ApexLat and the value reflects the quasi-dipole magnetic latitude (QD-Latitude) of its footprint in the ionospheric E-layer (110 km). Thus, measurements of Swarm A/C and Swarm B on the same field line appear at a common ApexLat. In this way, we can see, how the field-aligned plasma distribution spatially changes between the two spacecraft heights.

In support of the interpretation of these varying *Ne* differences between the two satellites, Figure 1b presents a schematical illustration of the field line and Swarm orbit configurations. Shown are the orbits of Swarm A and Swarm B (black dashed lines) and two magnetic field lines (blue solid lines) that have their apexes at Swarm A and Swarm B orbital heights. In addition, there is a fluxtube shown that goes up to a greater height. The presence of a plasma depletion region over a section of the fluxtube is marked by gray-shading. This fluxtube is sampled by Swarm A and B at different altitudes. The obtained quasi-simultaneous plasma density measurements can be used to estimate the scale length of EPB.

3 Observations

Figure 2 shows in the top frame electron density profiles derived by the three Swarm satellites from a pass of the equatorial region on 08 October 2021, shortly after 23:00 coordinated universal time (UTC) within the 20:00 MLT sector. The measurements from the closely spaced pair Swarm A/C are almost identical, while the quiet background *Ne* values at the higher altitude of Swarm B (green curve) are lower at low latitudes, but they seem to be higher near the equator. Clearly visible is the passage through a region containing several isolated plasma depletions near the magnetic equator. These are typical features of the F region irregularities during post-sunset hours. It is common practice to present such observations over QD-Latitude. However, the depletions are detected at quite different QD-Latitude by Swarm A/C and Swarm B. Conversely, for a more detailed inspection, in the lower frame of Figure 2 the *Ne* variations are plotted with respect to ApexLat. From this perspective, the detection of depletions is much better aligned between the spacecraft, and the background density is everywhere lower at Swarm B, as expected. All this confirms the suitability of the ApexLat frame for our study. There appears a data gap at low latitudes, due to the fact that E-region field lines near the magnetic equator do not reach up to the satellite altitudes. In the bottom panel, the magnetic longitude differences (ΔMLon) between the readings from Swarm A and Swarm B are plotted. It is

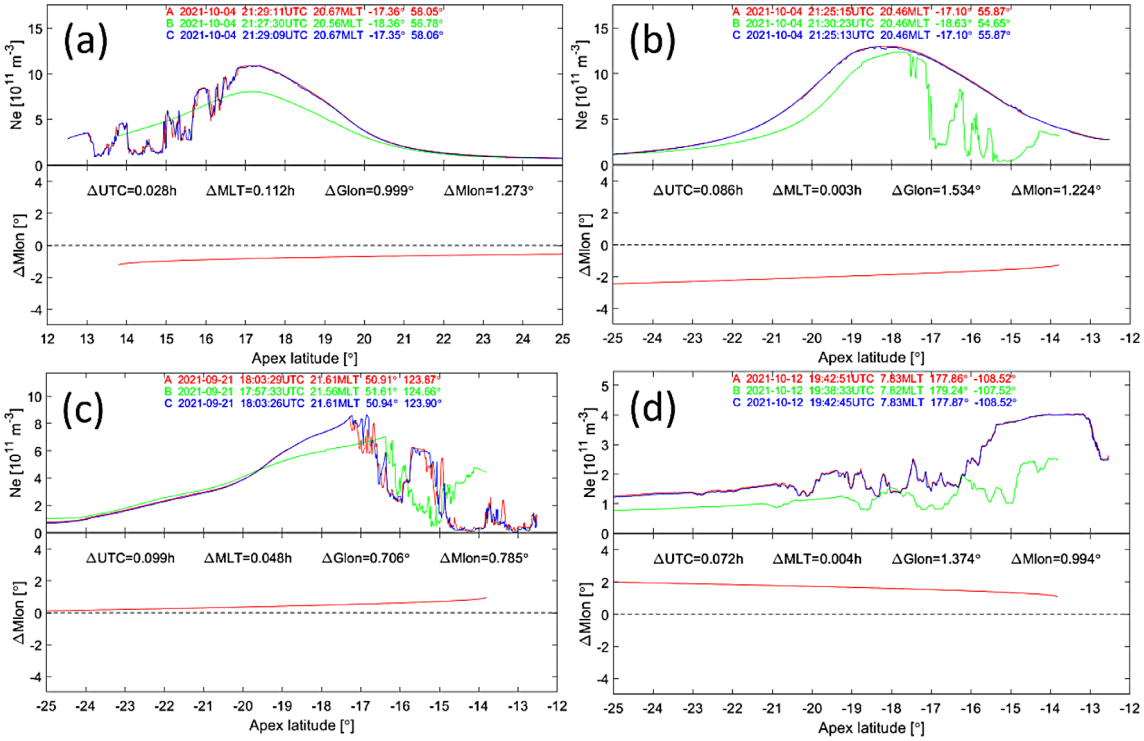

Figure 3. Examples of quasi-simultaneous observations of equatorial plasma bubbles by the three Swarm spacecraft. The listed times and locations of the spacecraft are valid at +15° or −15° ApexLat, depending on the hemisphere of the event.

known from previous studies (e.g. Huang et al., 2013; Xiong et al., 2016b; Xiong et al., 2018) that the longitudinal extent of EPBs can be small. Therefore, we limit our analysis to data segments of EPB that exhibit sufficiently small ΔMLon values.

3.1 Examples of plasma depletion events

Before going into a statistical evaluation of the plasma distribution along magnetic field lines we present a few typical examples. These events are suitable for explaining the interpretation approach and to introducing the criteria by which the ensemble of cases is characterized.

Figure 3 shows a collection of four different kinds of EPB configurations. General facts to note, during the considered period the Swarm B samples only fluxtubes down to 14° ApexLat, while the lower pair Swarm A/C reaches down to 12.5° ApexLat. Spacecraft times and locations listed at the top of the frames are valid at +15° or −15° ApexLat depending on the hemisphere presented. The example in frame (a) shows depletion signatures only recorded by the lower pair. No such signatures are observed by Swarm B flying 50 km higher, although all three spacecraft sample common fluxtubes at higher latitudes beyond 14° ApexLat. The opposite situation prevails in frame (b). Here only Swarm B observes depletion structures, while Swarm A/C at lower altitude detects no plasma irregularities on fluxtubes beyond 14° ApexLat. Already these two events, although fairly rare cases demonstrate that plasma depletions do not symmetrically extend over the whole fluxtube, but are limited to an upper or lower part of the fluxtube. A more common situation is depicted in frame (c). Over a range of apex latitudes all three spacecraft sense plasma depletions. But at a closer inspection differences become evident. Coming from higher latitudes, Swarm A/C senses irregularities from about −17.5° ApexLat, while Swarm B records plasma depletions only from latitudes one degree lower. That means the bubble occupies only the lower part of the fluxtube, below Swarm B. When moving further equatorward, Swarm A/C enters between −15° and −16° ApexLat an undisturbed region, while the *Ne* values at Swarm B are still depleted. This implies the bubble is confined to altitudes above Swarm A/C. Thereafter, depletions prevail down to the apex points of the related fluxtubes. This example also demonstrates the finite latitudinal sizes of depleted fluxtubes and the limited extension of the bubble along the magnetic field line. Finally, in frame (d) a case is presented where plasma irregularities extend to fairly high latitudes beyond −20° ApexLat. Such signatures seem to be caused by other processes different from EPBs. We think that they are related to medium-scale traveling ionospheric disturbances (MSTID) (e.g., Shiokawa et al., 2003; Park et al., 2009). These phenomena are commonly occurring at mid-latitudes but sometimes can reach down to low latitudes. We disregarded such unclear events from our statistics.

3.2 Statistical analysis of field-aligned depletion structure

After having seen four examples of plasma distributions simultaneously recorded on the same fluxtubes at two altitudes, we are now interested in the occurrence frequencies of the various types of depletion structures.

Before starting the analysis, we present the environmental conditions prevailing. The study period lasted from 5 September

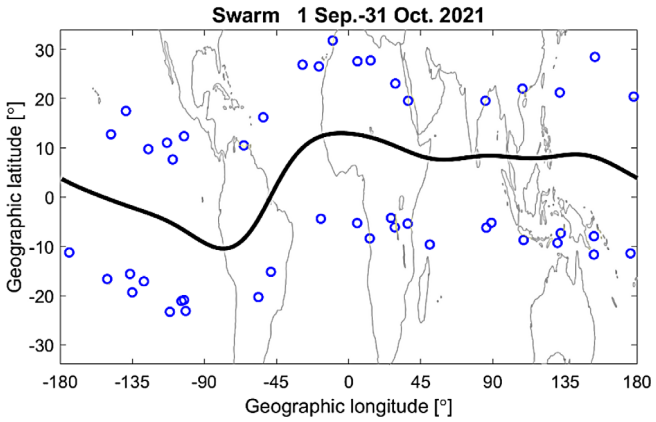

Figure 4. Distribution of the identified bubble events on a world map. Blue open circles mark ionospheric footprints (at 110 km altitude) of the poleward edges of the depleted fluxtubes.

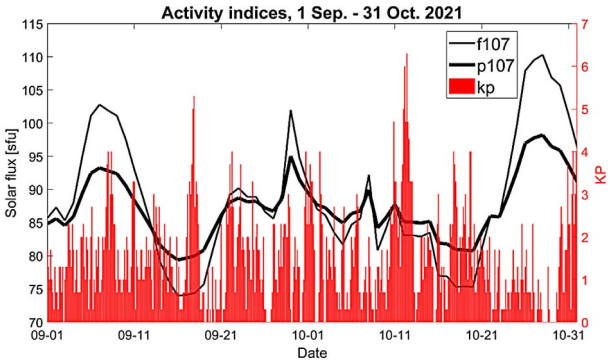

Figure 5. Evolution of activity indices during the two months of interest; the level of solar flux is reflected by the daily F10.7 and the smoother P10.7 and the magnetic activity by Kp.

to 17 October 2021. This overlaps with the fall season, which is known to be favorable for the appearance of EPBs at almost all longitudes (e.g., Burke et al., 2004; Stolle et al., 2006 and others). Limiting factors for our study period are the latitudes of Swarm A/C and B orbital crossing points and the magnetic local time of the cross-over, At the beginning (5 September 2021) the cross-over occurred around −25° ApexLat and at a local time of about 23:00 MLT. On 17 October 2021, the crossing reached about 20° ApexLat, but the local time had reduced to 19:30 MLT, which becomes unfavorable for EPBs (e.g., Stolle et al., 2006). Thereafter no suitable plasma depletion events have been detected although suitable constellations lasted until the end of October 2021. Almost simultaneous orbital crossings occurred about every 4 days, and last for about three consecutive orbits. For the event selection our initial requirements are: (i) the sample time difference between Swarm A/C and B shall not exceed 10 min; (ii) the difference of MLon must be below 1.5°; and (iii) there has to be clear signatures of plasma depletions. The criteria (i) and (ii) are checked at +15° and −15° ApexLat in the two hemispheres for validity, and (iii) has to be fulfilled somewhere within the range 12°–20° ApexLat. If all three are met in one hemisphere, that low-latitude arc is taken as an "event". With this selection approach, we identified 46 suitable events. This can be regarded as a reasonable number of events for a meaningful statistic. Figure 4 shows the distribution of identified events on a world map. Open circles mark ionospheric footprints of the poleward edges of depleted fluxtubes. We find a rather even distribution between the hemispheres, with 24 events in the southern and 22 in the northern hemisphere. Also, the events are quite evenly distributed over longitude. All this is consistent with the autumn longitudinal-seasonal characteristic of EPBs (e.g., Stolle et al., 2006; Xiong et al., 2010). We regard such an even spread of events as favorable for an unbiased statistical study.

For the interpretation of the mean EPB characteristics it is of interest to know the prevailing environmental conditions. Figure 5 presents the variation of some activity indices during the two months of interest. The evolution of solar flux is depicted in black lines, a thin line for the daily F10.7 index (e.g., Covington, 1947), and a heavy line for the somewhat smoother P10.7 values. P10.7 has been shown to better control the upper atmospheric processes (e.g., Liu et al., 2006) and used mainly in this study, which is defined as P10.7 = (F10.7 + F10.7A)/2, where F10.7A is the 81-day averaged value of the daily F10.7. Major solar flux peaks occurred on 7 September and about two solar rotations later on 27 October 2021. Otherwise, we observe a moderate solar flux level with P10.7 around 90 sfu. The *Kp* index (e.g., Bartels et al., 1939) is used to represent the magnetic activity, which is generally low during the considered period, with *Kp* = 4 being only exceeded on two days, 27 September and 12 October. For that reason, only minor influences from high-latitude processes are expected.

The set of events selected allows for a number of different interpretations. Here we start with the altitude at which the depletions occur. Swarm A/C visits the lowest fluxtube at its apex (see Fig. 1b at 435 km), which has an ionospheric footprint at 12.5° ApexLat. In 32 cases Swarm A/C encountered EPBs near the magnetic equator. This corresponds to a rate of 69%. On fluxtubes reaching apex heights between Swarm A/C and B orbit altitudes 34 bubble cases have been detected, amounting to a rate of 74%. Conversely, only 19 events (41%) are detected by Swarm B on fluxtubes touching its orbital height (506 km). This comparison shows that most of the bubbles can be found during this moderate activity period on fluxtubes reaching about 460 km altitude (~13° ApexLat).

Of particular interest for our goal to estimate the typical field-aligned length of EPBs are quasi-simultaneous observations by Swarm A/C and Swarm B on fluxtubes at latitudes beyond 14° ApexLat, which exceed the Swarm B height (see Fig. 1b). For this type of comparison, we have further tightened the selection criteria. Only common Swarm observations are separated by less than 1.0° in MLon. For the detection time difference we kept the 10 min limit. As justification, we have considered a maximal eastward propagation of the bubbles by about 100 m/s. Within 10 min this adds up to 60 km. For the sake of a sufficient number of events, we have not narrowed these limits any further. From our initial 46 events 28 are left for the bubble size estimation.

Figures 3a–3c show the three different kinds of EPB types that have been encountered. Cases where only Swarm A/C or Swarm B detects plasma depletions are rather rare, as presented in Figures 3a and 3b. The most common are the cases as shown in Figure 3c. Here we find partly common depletion signatures and sometimes effects only at one height. By visual inspection,

we went through all 28 events and classified the cases. The detections of depletions are unevenly distributed over the spacecraft: at Swarm A/C (18, 28%), at Swarm B (11, 17%), and simultaneously at both (35, 55%) (see Table 1, upper half). Only depletion structures larger than 0.5° ApexLat have been considered independent EPB fluxtubes. The listed sum exceeds the total number of 28 events because more than one class can be encountered during one pass.

For interested readers, plots of all 46 events are added as Supporting Information (SI) in a format as shown in Figure 3. Also, a Supplementary Table with an evaluation of the 28 considered events and in addition to using all 46 in the analysis, is enclosed there.

The rather moderate solar activity prevented the depleted fluxtube to expand to higher altitudes. Less than half the EPBs reached the orbital altitude of Swarm B. But for our analysis, only depletions on fluxtubes surpassing the height of Swarm B can be considered. In a recent study, Joshi et al. (2022) performed a detailed investigation of the peak height that a plasma bubble can be reached, depending on environmental conditions. They showed that the attained value depends on solar flux level and on local time. It takes up to about 22:00 local time until it stops rising. More important for the peak height is a high solar flux level, which is known to be accompanied by stronger vertical plasma drift (see e.g., Stolle et al., 2008; Su et al., 2008; Joshi et al., 2022). For a solar flux level of P10.7 about ~90 sfu, as prevailing during our study period, Joshi et al. (2022) derived a median peak height of about 550 km within the 80° W–10° E longitude sector. The global EPB occurrence distribution obtained from CHAMP and GRACE observations (Xiong et al., 2010) showed that it is just this American sector where larges fluxtube heights do occur. When considering the global distribution of our events and the local time range 19:30–23:00 LT the median fluxtube height of 460 km, obtained here, can be regarded as consistent with the result of Joshi et al. (2022). It would have been more favorable for our analysis to have solar flux values of e.g., 150 sfu for P10.7. In that case, the mean peak heights could be expected about 200 km higher and many more common bubble detections should have been available.

Concerning magnetic activity, the generally quiet periods ensured clear EPB signatures. Only on two days within our study period $Kp = 5$ were reached (17 September and 12 October). This enhanced activity resulted in some irregular signals for our analysis. For example, on 17 September depleted plasma density appeared at 20° ApexLat and beyond (see SI pages 38 and 40). Differently, in the case of 12 October, irregular plasma variations were observed, which look different from EPBs (see SI pages 34 and 37). We interpreted them as middle latitude MSTID (e.g., Shiokawa et al., 2003). In Table S1 these events are marked by "MST". Similar MST events were also observed on 13 September (SI pages 27 and 33). Under certain conditions the MST events can obviously travel down to low latitudes. For our scale analysis we did not consider any of these special plasma variations.

4 Discussion

EPBs usually contain plasma density structures with transverse scales from sub-meter to over several hundred kilometers (e.g., Yokoyama et al., 2014), but less is known about their actual field-aligned lengths. Therefore, their 3-D structure is still of interests for the scientists. However, due to the lack of simultaneous measurements at multi-points for one and the same EPB, it is not easy to reliably derive the scale-length, especially for the finer structures. By correlating the *Ne* profiles along satellite tracks of Swarm during the initial mission phase, when the separation of Swarm gradually increases, Xiong et al. (2016b) reported a typical zonal extent of 50 km for smaller EPBs. Such a zonal extend is consistent with the airglow image observations (e.g., Wu et al., 2017). Different to Xiong et al. (2016b), in this study we try to resolve the field-aligned scale length of EPBs, which needs simultaneous measurements along the same fluxtube but at different altitudes. The Swarm counter-rotation constellation with Swarm A/C and Swarm B flying on quasi-coplanar orbits provides a good opportunity for addressing this issue. Though the number of EPB events considered is not large, we think our concept and statistical results are meaningful due to the quite strict criteria concerning temporal and spatial separation between Swarm A/C and B measurements.

Table 1. Results of field-aligned bubble scale-length estimate based on simultaneous observations of plasma depletions on the same fluxtubes by either one or both Swarm spacecraft. The rows in the upper halve list the numbers of either single-satellite EPB detections by Swarm A or B and the double detections at the various fluxtubes from the considered 28 events. In the lower part the values of parameters for calculating the scale length, *L*, are listed (see Eq. (4) for the definition).

	Apex latitude of fluxtube				
	18°	17°	16°	15°	14°
Swarm A	2	2	4	5	5
Swarm B	0	0	1	5	5
Swarm A + B	4	5	8	7	11
Sum	6	7	13	17	21
p	0.67	0.71	0.62	0.41	0.52
a	3.0	3.45	2.6	1.7	2.1
d (km)	170	190	223	283	485
L (km)	510	655	579	481	1018

Early airglow observations provided evidence of long field-aligned dark bands of plasma depletions which could be associated with EPBs (e.g., Mendillo et al., 1997). These images suggested depletions extending practically over the whole fluxtube. However, more recent observation and model results suggested, as outlined in the Introduction, that individual plasma bubbles sometimes occupy only part of the fluxtube. This inference is well confirmed by the Swarm simultaneous observations on the same fluxtube but at two altitudes. Several of the bubbles are only detected by one Swarm spacecraft at a time. Such single-spacecraft observations alone, however, are not too helpful for making quantitative estimates of bubble length. Equally suitable are cases where Swarm A/C and Swarm B both detected the depletion on the same fluxtube. These together allow to estimate the field-aligned length of bubbles.

In Figure 1b we see that the spacecraft Swarm A and B (here and in the following we use only the letter A when talking about the pair A/C) sample the electron density on the same field line at a distance, *d*, from each other. This distance gets

longer, the closer the spacecraft come to the equator. The value of d can be calculated with the help of the cosine theorem:

$$d^2 = r_A^2 + r_B^2 - 2\, r_A\, r_B \cos(\Delta ß), \tag{1}$$

where r_A = 6813 km and r_B = 6884 km are typical radial distances of Swarm A and B during the time period of counter-rotation; $\Delta\beta$ is the difference in magnetic latitude of the spacecraft when they sample the same fluxtube at their two altitudes, $\Delta\beta = \beta_A - \beta_B$. Each field line is identified by its ApexLat, β_{Ion}. By assuming a dipole field geometry, the magnetic latitude corresponding to an ApexLat can be computed for both spacecraft:

$$\cos^2(ß_A) = \frac{r_A}{r_{\mathrm{Ion}}} \cos^2(ß_{\mathrm{Ion}}), \tag{2}$$

$$\cos^2(ß_B) = \frac{r_B}{r_{\mathrm{Ion}}} \cos^2(ß_{\mathrm{Ion}}), \tag{3}$$

where the radial distance of the ionosphere near the equator is taken to be r_{Ion} = 6488 km (110 km height). Figure 6 shows the resulting field line length, d, between the Swarm satellites, as it varies with ApexLat. This clearly shows that the distance is progressively increasing the closer the satellites come to lower ApexLat. At 20° ApexLat it starts around 150 km, and the field line length reaches 500 km when Swarm B reaches the apex point of the 14° ApexLat fluxtube.

For obtaining a quantitative estimate of the typical plasma bubble length we may consider a simple statistical game. Imagine two sensors separated by a distance d in a 1D setup. Take a stick of length L and drop it randomly onto the line connecting the two sensors. Record the events when the stick touches one or both sensors. In the case of $L < d$ there will be no double-responses. If L approaches an infinite length, the two sensors will always respond. Of interest here are cases with a finite L that is larger than the distance d. For the mentioned statistical game, we can express the probability, p, for a double-response

$$p = \frac{N_{\mathrm{double}}}{N_{\mathrm{single}} + N_{\mathrm{double}}} = \frac{(a-1)}{a}, \tag{4}$$

where N_{single} and N_{double} are the number of hits of a single or both sensors; $a = \dfrac{L}{d}$ is the ratio between the length of the stick and the distance between sensors. Also here, it is obvious that a has to be larger than 1, in order to obtain a sensible probability. By counting the individual bubble detections of Swarm A and Swarm B and considering the common bubble detections we can make use of equation (4). With some reordering we get:

$$a = \left(1 - \frac{N_{\mathrm{double}}}{N_{\mathrm{single}} + N_{\mathrm{double}}}\right)^{-1}. \tag{5}$$

In a next step we calculate $L = a \cdot d$ to estimate the typical length L of the depleted fluxtube part. Since the length of the fluxtube segment, d, between the satellite encounters varies with latitude, we determined the detection counts separately at 14°, 15°, 16°, 17°, and 18° ApexLat. The obtained results are listed in Table 1. The count rates are rather low, in particular for the higher reaching fluxtubes. This is partly caused by the concentration of EPB events on lower apex fluxtubes and by our restriction to events obeying the strict Swarm A and B detections criteria.

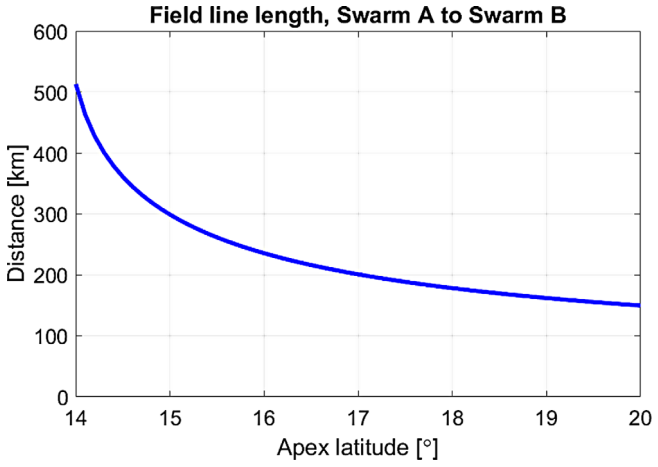

Figure 6. Length of field line segment between the orbits of Swarm A and B, depending on the ApexLat of the fluxtube.

A-priori, we have no information about the bubble scale length L, but we need to know, for the interpretation, whether d is smaller than L or not. For that reason, we started the interpretation of derived L values in Table 1 from the high-latitude end, where field-aligned spacecraft separations are smallest and the condition, $d < L$ best fulfilled. Within the latitude range 15°–18° ApexLat we find rather consistently values for L between 481 and 655 km. Differently, at lower latitudes (e.g. 14° ApexLat) a significantly larger length is obtained. This L value is considered unrealistic. Our explanation for that result is that the field-aligned separation, d, between Swarm A and B becomes too large at that low latitude, so the requirement of $L > d$ is no longer always fulfilled. That means, double detections are not only caused by the same bubble but also by two separate depletions. Therefore, they occur too frequently and the analysis results in a too large parameter, a.

In addition, for test purposes, we have extended our EPB scale-length estimates to the full set of the 46 events, where the allowed longitudinal separation between Swarm A and Swarm B goes up to 1.5° MLon. Results of that analysis are listed in the Supplement Information as part of Table S1, the numbers in parenthesis. The derived scale length, L, are systematically smaller than the original ones. This demonstrates that the length estimates tend to underestimate the bubble size when the longitudinal distance between simultaneous *Ne* measurements is too large. In those cases, some of the expected double detections have obviously been missed.

For a better interpretation of the derived bubble scale length we may compare it with the whole length of a fluxtube. This can conveniently be calculated. When assuming dipole geometry for the field lines, at low latitudes they can reasonably well be approximated by a circle with radius of one-third of the distance from the apex point to the Earth center. Assuming a start height of 150 km for the affected fluxtube, we get, e.g. for the 16° ApexLat line a length of 3840 km (14° ApexLat: 3267 km, 18° ApexLat: 4455 km). This is 6 times longer than our mean estimated length of about 550 km. We may thus suggest that there are several individual plasma bubbles along a fluxtube.

According to the Table 1, there are several cases where only Swarm A detected a depletion. Such examples can also be used for validating the derived finite field-aligned length. In those

cases, the bubble has to fit into the fluxtube part below Swarm B. By employing equation (1), it is possible to calculate the arc length of the fluxtube from 150 km to the orbit of Swarm B. The distance increases the closer the field lines are to the equator. For the 18° ApexLat line we get 640 km and for 17° ApexLat 710 km (16° ApexLat: 800 km, 15° ApexLat: 945 km, 14° ApexLat: 1265 km). These length values can be regarded as an upper limit for the single-spacecraft bubble detections by Swarm A, and our scale-length estimates fit well into the fluxtube arc below Swarm B at 18° ApexLat. Also, the increasing number of single Swarm A detections towards lower apex latitudes goes well with the increasing arc length.

In a recent paper, Ghadjari et al. (2022) deduced for two plasma bubble events a length of 100–200 km from standing Alfvén wavelength estimates inside the depleted volume. These numbers are much lower than our results. However, it has to be taken into account that they had chosen two very narrow EPB structures close to the magnetic equator, where we have no events. Conversely, we had requested a minimum size of 0.5° ApexLat for our events. This may be a reason for their much smaller length compared to our estimates of order 500–600 km bubble extensions. Our derived typical field-aligned lengths of plasma depletion are at least valid in the range of the equatorial ionization anomaly and at the lower part of the fluxtube. For fluxtubes at 14° ApexLat and below we cannot provide estimates because the spacecraft separation, d, becomes too large.

Our estimates of finite depleted sections along a fluxtube seem to be in contrast with some of the EPBs in airglow observations, showing long dark bands along magnetic meridian. A way to reconcile the two apparently conflicting observations may be to assume several depleted fluxtubes within the same meridional plane, but at different apex heights, which are placed above each other. As a result, the superposed depletions appear in the airglow images as continuous bands. In any way, there have been several independent reports about finite lengths of EPBs in the literature as outlined in the Introduction.

Finally, we want to stress that the Swarm counter-rotation constellation period with Swarm A/C and Swarm B flying on quasi-coplanar orbits has provided a unique chance to investigate the scale-length of EPBs. There has never before been such an opportunity, and there is no second chance for a comparable study in sight. Although the number of suitable EPB events is not large, 46 (28) probably too small for a significant statistic, we think it would be a pity when the results of our serious try had not been made public. The consistent results of bubble scale-lengths obtained by applying our approach to the five independent fluxtubes adds to the confidence in the derived values. We leave it to the readers to decide themselves, what are their take-home messages from this study.

5 Summary and Conclusions

In this study, we make use of the Swarm counter-rotation constellation for estimating the typical scale length of depleted EPBs along the fluxtube. We are fortunate that the close approaches between the Swarm spacecraft near the equator occurred during local times from 19:00 to 23:00 MLT, when the plasma irregularities prefer to build up. Also the season, September and October, is favorable for the even occurrence of EPBs around the globe. Our observations provide clear evidence for a finite extension of the depleted section within a fluxtube. Main findings can be summarized as follows:

1. EPBs are observed preferably during these times of moderate solar and magnetic activity on fluxtubes that do not exceed much the altitude of the Swarm A/C orbit (435 km), while Swarm B (at 506 km) detects already significantly less bubbles. This is consistent with the height-dependence of EPB occurrence frequencies obtained from CHAMP and GRACE observations (Xiong et al., 2010) and in line with the peak-height results presented by Joshi et al. (2022) for similar solar flux levels.
2. Quasi-simultaneous sampling by Swarm A/C and Swarm B of the same fluxtube frequently results in depletion detections at only one spacecraft, confirming that plasma bubbles tend to extend only over a finite part of the fluxtube.
3. A statistical analysis of the double and single bubble detections on common fluxtubes reveals a typical field-aligned length of the depletions of the order of 550 km at the 15°–18° ApexLat field lines. Our sampled region overlaps well with the lower part of the fluxtube within the equatorial ionization anomaly. In the near-equatorial region and top part of the fluxtube we cannot make length estimates.
4. At fluxtubes of 14° ApexLat and more equatorward, our length estimate breaks down because of too large spacecraft spacing between Swarm A/C and B. This is somewhat unfortunate because the highest EPB occurrence rates were found around 13° ApexLat. A higher solar flux level or a smaller difference in orbit altitudes (e.g., 20 km above Swarm A) would be needed for extending our scale analysis to the favorable fluxtubes.

Presently we do not have a conclusive explanation for the process causing the reported size of bubble length. Speculation could be that the ionospheric instability, causing the rising plasma depletions, works intermittently thus creating separated bubbles in the fluxtube. Dedicated model simulations are probably needed for clarifying those conditions.

Acknowledgements. This work is supported by the Special Fund of Hubei Luojia Laboratory (220100011) and the National Natural Science Foundation of China (42174191). The Swarm data are provided by ESA at the website: https://earth.esa.int/web/guest/swarm/data-access. The solar flux index F10.7 is available at the OMNIWeb database https:// omniweb.gsfc.nasa.gov/, and the *Kp* index is available at the GFZ German Research Centre for Geosciences (https://www.gfz-potsdam.de/en/section/geomagnetism/data-products-services/geomagnetic-kp-index). The editor thanks two anonymous reviewers for their assistance in evaluating this paper.

Supplementary materials

The supplementary information of this article is available at https://www.swsc-journal.org/10.1051/swsc/2023002/olm.

Table S1: Complete list of all considered EPB events during the Swarm counter-rotation period. In the middle part the detection of plasma depletions either by Swarm A, Swarm B or by both is marked for every degree of ApexLat. In some places "MST" mark the appearance of Medium-Scale Traveling Ionospheric Disturbances rather than plasma bubbles.

Table S2: Evaluation of bubble scale-length based on simultaneous observations of plasma depletions on the same fluxtubes by either one or both Swarm spacecraft. The columns contain results obtained from fluxtubes labelled by their apex latitude. The rows in the upper half list either the numbers of single-satellite EPB detections by Swarm A or B, below the double detections and the Sum at the various fluxtubes from the considered 28 prime events. In the lower part the values of parameters for calculating scale-length are listed (for definition see Eq. (4) in parent paper). The bottom row presents the estimates for the field-aligned bubble lengths. All numbers in parenthesis are derived from the full set of 46 EPB events allowing for longitudinal separations up to 1.5° ΔMLon.

Figure S1: Increase of available events for the scale-length study with a growing range of allowed difference in magnetic longitude, ΔMLon, between Swarm A and B EPB detections.

Figure S2: (46 frames). For all the considered events the quasi-simultaneous observations of equatorial plasma bubbles by the three Swarm spacecraft are shown. The listed times and locations of the spacecraft are valid for + or −15° ApexLat, depending on the hemisphere.

References

Bartels J, Heck N, Johnston H. 1939. The three-hour-range index measuring geomagnetic activity. *Terr Magn Atmos Electr* **44(4)**: 411–454. https://doi.org/10.1029/te044i004p00411.

Burke WJ, Gentile LC, Huang CY, Valladares CE, Su SY. 2004. Longitudinal variability of equatorial plasma bubbles observed by DMSP and ROCSAT-1. *J Geophys Res* **109**: A12301. https://doi.org/10.1029/2004JA010583.

Covington AE. 1947. Microwave solar noise observations during the eclipse of November 23, 1946. *Nature* **159**: 405–406.

Dao E, Seyler C, Kelley M. 2013. Three-dimensional modeling of the electromagnetic characteristics of equatorial plasma depletions. *J Geophys Res Space Phys* **118(6)**: 3505–3514. https://doi.org/10.1002/jgra.50216.

Emmert JT, Richmond AD, Drob DP. 2010. A computationally compact representation of Magnetic-Apexand Quasi-Dipole coordinates with smooth base vectors. *J Geophys Res* **115**: A08322. https://doi.org/10.1029/2010JA015326.

Fejer BG, Scherliess L, de Paula ER. 1999. Effects of the vertical plasma drift velocity on the generation and evolution of equatorial spread F. *J Geophys Res* **104**: 19859–19869. https://doi.org/10.1029/1999JA900271.

Friis-Christensen E, Lühr H, Knudsen D, Haagmans R. 2008. Swarm – An Earth observation mission investigating. *Geospace Adv Space Res* **41**: 210–216. https://doi.org/10.1016/j.asr.2006.10.008.

Ghadjari H, Knudsen D, Skone S. 2022. Standing Alfvén waves within equatorial plasma bubbles. *Geophys Res Lett* **49(7)**. e2021GL097526. https://doi.org/10.1029/2021GL097526.

Heelis R, Kendall P, Moffett R, Windle D, Rishbeth H. 1974. Electrical coupling of the E-and F-regions and its effect on F-region drifts and winds. *Planet Space Sci* **22(5)**: 743–756. https://doi.org/10.1016/0032-0633(74)90144-5.

Huang C-S, de La Beaujardière O, Roddy PA, Hunton DE, Ballenthin JO, Hairston MR, Pfaff RF. 2013. Large-scale quasiperiodic plasma bubbles: C/NOFS observations and causal mechanism. *J Geophys Res Space Phys* **118**: 3602–3612. https://doi.org/10.1002/jgra.50338.

Huang C-S, Le G, de La Beaujardiere O, Roddy PA, Hunton DE, Pfaff RF, Hairston MR. 2014. Relationship between plasma bubbles and density enhancements: Observations and interpretation. *J Geophys Res Space Phys* **119**: 1325–1336. https://doi.org/10.1002/2013JA019579.

Joshi DR, Groves KM, Retterer JM, Carrano CS, Roddy PA. 2022. Peak-height distribution of equatorial ionospheric plasma bubbles: Analysis and modeling of C/NOFS satellite observations. *J Geophys Res Space Phys* **127**: e2022JA030525. https://doi.org/10.1029/2022JA030525.

Kelley MC. 2009. *The Earth's ionosphere, plasma physics and electrodynamics*, 2nd edn. Academic, San Diego, CA.

Kil H, Heelis RA, Paxton LJ, Oh S-J. 2009. Formation of a plasma depletion shell in the equatorial ionosphere. *J Geophys Res* **114**: A11302. https://doi.org/10.1029/2009JA014369.

Kintner PM, Ledvina BM, de Paula ER. 2007. GPS and ionospheric scintillations. *Space Weather* **5**: S09003. https://doi.org/10.1029/2006SW000260.

Knudsen D, Burchill J, Buchert S, Eriksson A, Gill R, Wahlund J-E, Åhlen L, Smith M, Moffat B. 2017. Thermal ion imagers and Langmuir probes in the swarm electric field instruments. *J Geophys Res Space Phys* **122(2)**: 2655–2673. https://doi.org/10.1002/2016JA022571.

Le G, Huang C-S, Pfaff RF, Su S-Y, Yeh H-C, Heelis RA, Rich FJ, Hairston M. 2003. Plasma density enhancements associated with equatorial spread F: ROCSAT-1 and DMSP observations. *J Geophys Res* **108**: 1318. https://doi.org/10.1029/2002JA009592.

Liu L, Wan W, Ning B, Pirog OM, Kurkin VI. 2006. Solar activity variations of the ionospheric peak electron density. *J Geophys Res* **111**: A08304. https://doi.org/10.1029/2006JA011598.

Luo X, Xiong C, Gu S, Lou Y, Stolle C, Wan X, Liu K, Song W. 2019. Geomagnetically conjugate observations of equatorial plasma irregularities from Swarm constellation and ground-based GPS stations. *J Geophys Res Space Phys* **124**: 3650–3665. https://doi.org/10.1029/2019JA026515.

Mendillo M, Baumgardner J, Nottingham D, Aarons J, Reinisch B, Scali J, Kelley M. 1997. Investigations of thermospheric-ionospheric dynamics with 6300-Å images from the Arecibo Observatory. *J Geophys Res* **102(A4)**: 7331–7343. https://doi.org/10.1029/96JA02786.

Mukherjee GK, Carlo L, Mahajan SH, Patil PT. 1998. First results of all-sky imaging from India. *Earth Planet Space* **50(2)**: 119–127. https://doi.org/10.1186/BF03352093.

Park J, Lühr H, Stolle C, Rother M, Min KW, Chung J-K, Kim YH, Michaelis I, Noja M. 2009. Magnetic signatures of medium-scale traveling ionospheric disturbances as observed by CHAMP. *J Geophys Res* **114**: A03307–A12345. https://doi.org/10.1029/2008JA013792.

Pimenta AA, Bittencourt JA, Fagundes PR, Sahai Y, Buriti RA, Takahashi H, Taylor MJ. 2003. Ionospheric plasma bubble zonal drifts over the tropical region: A study using OI 630 nm emission all-sky images. *J Atmos Sol Terr Phys* **65(10)**: 1117–1126. https://doi.org/10.1016/S1364-6826(03)00149-4.

Shiokawa K, Otsuka Y, Ihara C, Ogawa T, Rich FJ. 2003. Ground and satellite observations of nighttime medium-scale traveling

ionospheric disturbance at midlatitude. *J Geophys Res* **108(A4)**: 1145. https://doi.org/10.1029/2002JA009639.

Stolle C, Lühr H, Rother M, Balasis G. 2006. Magnetic signatures of equatorial spread F, as observed by the CHAMP satellite. *J Geophys Res* **111**: A02304. https://doi.org/10.1029/2005JA011184.

Stolle C, Lühr H, Fejer BG. 2008. Relation between the occurrence rate of ESF and the equatorial vertical plasma drift velocity at sunset derived from global observations. *Ann Geophys* **26**: 3979–3988. https://doi.org/10.5194/angeo-26-3979-2008.

Su S-Y, Chao CK, Liu CH. 2008. On monthly/seasonal/longitudinal variations of equatorial irregularity occurrences and their relationship with the postsunset vertical drift velocities. *J Geophys Res* **113**: A05307. https://doi.org/10.1029/2007JA012809.

Wu K, Xu J, Wang W, Sun L, Liu X, Yuan W. 2017. Interesting equatorial plasma bubbles observed by all-sky imagers in the equatorial region of China. *J Geophys Res Space Phys* **122**: 10596–10611. https://doi.org/10.1002/2017JA024561.

Xiong C, Park J, Lühr H, Stolle C, Ma SY. 2010. Comparing plasma bubble occurrence rates at CHAMP and GRACE altitudes during high and low solar activity. *Ann Geophys* **28**: 1647–1658. https://doi.org/10.5194/angeo-28-1647-2010.

Xiong C, Stolle C, Lühr H. 2016a. The Swarm satellite loss of GPS signal and its relation to ionospheric plasma irregularities. *Space Weather* **14**: 563–577. https://doi.org/10.1002/2016SW001439.

Xiong C, Stolle C, Lühr H, Park J, Fejer BG, Kervalishvili GN. 2016b. Scale analysis of equatorial plasma irregularities derived from Swarm constellation. *Earth Planet Space* **68**, 1–12. https://doi.org/10.1186/s40623-016-0502-5.

Xiong C, Xu J, Wu K, Yuan W. 2018. Longitudinal thin structure of equatorial plasma depletions coincidently observed by Swarm constellation and all-sky imager. *J Geophys Res Space Phys* **123**: 1593–1602. https://doi.org/10.1002/2017JA025091.

Yeh KC, Liu CH. 1982. Radio wave scintillations in the ionosphere. *Proc IEEE* **70**: 324–360.

Yokoyama T, Shinagawa H, Jin H. 2014. Nonlinear growth, bifurcation, and pinching of equatorial plasma bubble simulation by three-dimensional high-resolution bubble model. *J Geophys Res Space Phys* **119**: 10474–10482. https://doi.org/10.1002/2014JA020708.

Cite this article as: Xiong C & Lühr H 2023. Field-aligned scale length of depleted structures associated with post-sunset equatorial plasma bubbles. *J. Space Weather Space Clim.* **13**, 3. https://doi.org/10.1051/swsc/2023002.